PROSPECTS
IN PHARMACEUTICAL SCIENCES

Prospects in Pharmaceutical Sciences, -
https://prospects.wum.edu.pl/

Original Article

From Tradition to Mechanism: Anti-inflammatory and Microbiota-Modulating Effects of *Calendula officinalis* and *Matricaria recutita* Extracts on the Skin

Natalia Melnyk[1], Weronika Skowrońska[1], Dominik Popowski[1,2], Jakub Piwowarski[3], Sebastian Granica[1,*]

[1] *Department of Pharmaceutical Biology, Faculty of Pharmacy, Medical University of Warsaw, Banacha 1, 02-097, Warsaw, Poland*

[2] *Department of Food Safety and Chemical Analysis, Waclaw Dabrowski Institute of Agricultural and Food Biotechnology-State Research Institute, Warsaw, Poland*

[3] *MicrobiotaLab, Department of Pharmaceutical Microbiology and Bioanalysis, Medical University of Warsaw, Banacha 1, Warsaw, Poland*

* Correspondence, e-mail: Sebastian Granica, Department of Pharmaceutical Biology, Faculty of Pharmacy, Medical University of Warsaw, Banacha 1, 02-097 Warsaw, Poland, tel/fax +48 22 5720953, e-mail: sgranica@wum.edu.pl

Received: 27.10.2025 / Revised: 01.12.2025 / Accepted: 01.12.2025 / Published: 11.12.2025

ABSTRACT

The skin represents a complex ecosystem where host cells and microbiota coexist in dynamic equilibrium. Disruption of this balance contributes to inflammation and diseases, while natural compounds may help restore it. For centuries, marigold and chamomile have been among the most valued medicinal plants in traditional herbal medicine, widely used for treating wounds, skin inflammation, and irritations. Their long-standing therapeutic reputation is supported by rich phytochemical profiles – triterpenoids, flavonoids, phenolic acids in marigold, and sesquiterpene lactones, flavonoids, and coumarins in chamomile – known to exert anti-inflammatory, antioxidant, and soothing effects. In this study, *Calendula officinalis* and *Matricaria recutita* flower extracts' effects were investigated on human skin microbiota and dermal cells. Both extracts remained chemically stable under microbial exposure and did not generate new metabolites, highlighting resistance to microbial metabolism. Neither extract disrupted community structure; instead, they selectively modulated microbial taxa, decreasing potentially pro-inflammatory families (*Staphylococcaceae*, *Corynebacteriaceae*, and *Enterococcaceae*) and enriching *the Bacillales and Bacillaceae* families. On the cellular level, at ≤250 µg/mL, both extracts were biocompatible with fibroblasts and keratinocytes. Marigold flower extract showed no significant anti-inflammatory effect in keratinocytes, as IL-6 and IL-8 secretion remained comparable to the stimulated control. In contrast, Chamomile flower extract markedly reduced IL-6 levels in a dose-dependent manner, with moderate effects on IL-8. In fibroblasts, both extracts had strong suppression of IL-6 and IL-8 at higher concentrations. These findings reveal a dual mechanism – direct cellular modulation and indirect microbiota-mediated rebalancing-supporting the traditional therapeutic efficacy of *C. officinalis* and *M. recutita* in skin health.

KEYWORDS: Calendula officinalis, Matricaria recutita, skin microbiota, inflammation

1. Introduction

Skin conditions are a major public health concern, affecting 30–70% of the global population. They are the most common reason for visits to general practitioners. Over 3,000 different skin disorders, both acute and chronic, have been identified, affecting people of all ages and socioeconomic levels [1]. A lot of studies show that skin conditions can significantly alter the microbiota's diversity and composition. For example, in human and animal patients with atopic dermatitis, dysbiosis of the skin microbiota leads to decreased diversity of microbial populations. It is unclear whether these altered microbial populations are the cause or effect of inflammatory skin conditions observed in humans and animals, but there is no doubt that the microbiome plays an important role in skin health. Also, research is growing on how the human microbiome works with exogenous exposures and the body to create a homogenous environment promoting

ultimate health [2].

At the cellular level, keratinocytes and dermal fibroblasts are key players in skin health and disease. Keratinocytes, which constitute the majority of the epidermis, act as the first line of defense against environmental stimuli, releasing cytokines and antimicrobial peptides that orchestrate the immune response [3]. Dermal fibroblasts, embedded in the connective tissue of the dermis, contribute to tissue repair and extracellular matrix remodeling but also secrete mediators that modulate inflammation [4]. Together, these cell types not only respond to exogenous factors but also shape the local microenvironment in which the microbiota resides. Thus, understanding how external interventions – such as natural plant extracts – interplay with cell and microbial communities is crucial for developing innovative therapeutic strategies.

Medicinal plants have a remarkable history of benefiting humanity across nearly every continent. Natural products are essential sources for drug discovery, and many contemporary topically applied medications used in modern pharmacotherapy have their origins in traditional herbal medicine [5]. Medicinal plants still hold great promise for the future, as the phytochemical composition and potential health benefits of numerous species remain unexplored or require further in-depth research [6]. In recent years, there has been growing interest in natural alternatives to synthetic anti-inflammatory agents [7]. Plant extracts, traditionally used in folk medicine for their healing properties, have gained significant attention in dermatological research due to their bioactive compounds that can modulate inflammatory processes [8,9].

Among the most recognized medical herbs used in topical formulations are *Calendula officinalis* L. (marigold) and *Matricaria recutita L.* (chamomile), both officially listed in pharmacopeias and valued for their long-standing use in treating skin inflammation, wounds, and irritations. Marigold is rich in triterpenoids, flavonoids, carotenoids, and phenolic acids, which contribute to its anti-inflammatory, antimicrobial, and wound-healing activities [10]. Chamomile, on the other hand, contains a complex of sesquiterpene lactones (chamazulene, α-bisabolol, matricin), flavonoids (apigenin, luteolin, quercetin glycosides), and coumarins, which collectively exhibit anti-inflammatory, antioxidant, and soothing effects [11]. Chamomile preparations are known to interfere with NF-κB signaling and to downregulate interleukin expression, thus attenuating the inflammatory response associated with various dermatoses [12]. Both species have been incorporated into numerous dermatological and cosmetic preparations designed to restore skin homeostasis, reduce erythema, and support tissue regeneration. Despite their widespread use, the precise mechanisms of action remain insufficiently characterized. Moreover, the interactions between plant materials and the skin are multifaceted. On one hand, plant compounds can influence skin cells, promoting healing, reducing inflammation, and modulating immune responses. On the other hand, these compounds may interact with the skin's microbiota - the diverse community of microorganisms that live on the skin's surface and play a key role in protecting against pathogens, modulating inflammation, and maintaining skin barrier function. Recent studies highlight that this interaction is bidirectional. Phytochemicals can selectively influence microbial growth, inhibit pathogenic bacteria, and promote beneficial commensals, thereby balancing dysbiotic communities [13]. In turn, microorganisms can metabolize plant-derived compounds into bioactive derivatives with altered or enhanced biological activity [14,15].

Taken together, skin health emerges as a dynamic outcome of the interplay between cells, microbiota, and exogenous bioactive compounds, with medicinal plants offering a unique bridge between traditional practices and modern scientific approaches.

The main objective of this work is to evaluate how traditionally used *Calendula officinalis* and *Matricaria recutita* extracts interplay with skin microbiota, as well as their influence on keratinocytes and dermal fibroblasts. Given that the mechanism of action of plant-derived preparations is still not fully elucidated, this approach – combining cellular models with microbiota studies – will contribute to a more comprehensive understanding of how these materials exert their effects. In particular, it will clarify how microbial metabolism may influence the chemical composition of marigold and chamomile extracts, thereby influencing their efficacy and biological relevance.

2. Materials and Methods

The interactions of a 70% (*v*/*v*) ethanolic extracts with human skin microbiota were studied. The impact of a 70% (*v*/*v*) ethanolic extracts on the inflammatory response in skin cells (including fibroblasts and keratinocytes) were examined. The chemical composition of the extracts was characterized using UHPLC-DAD-MS^n.

2.1. Plant sources and extraction

Calendulae officinalis flos and *Matricariae recutita flos* (batch numbers: 2079 and 911.2019, expiration dates: July 2020 and September 2020, respectively) were obtained from Kawon-Hurt (Gostyn, Poland) and Flos (Mokrsko, Poland), respectively. A voucher specimen has been cataloged in the Herbarium of the Department of Pharmaceutical Biology at the Medical University of Warsaw, Poland, under the reference numbers 2020CO07 and 2020CH09. The plant materials were identified as marigold and chamomile flowers through macroscopic and microscopic analysis conducted by Prof. Sebastian Granica, following the methods described by European Pharmacopeia monographs. Additionally, TLC analysis was performed to confirm the plant's identity and compliance with the manufacturer's specifications [16,17].

A total of 50 g of plant material (*C. officinalis flos* or *M. recutita flos*) was subjected to triple extraction with 500 mL of 70% ethanol (*v*/*v*, 7:3) at room temperature under periodic stirring. To improve compound recovery, each extraction step included 15 minutes of ultrasonic bath treatment. The combined extracts were filtered and concentrated under reduced pressure (<45 °C) using a LABORANTA 4000 WB vacuum system (Heidolph, Schwabach, Germany). The concentrate was frozen at −20 °C for 24 h and subsequently lyophilized in a Cryodos freeze-dryer (Telstar, Terrassa, Spain). This process yielded 14,45 g of MFE (marigold flower extract) and 4,04 g of CFE

(chamomile flower extract), which were stored in an airtight container at 4 °C until use.

For analysis, the dry extract was dissolved in MeOH to prepare a 10 mg/mL solution for UHPLC-DAD-MS^n analysis, a 12 mg/mL solution in H_2O was prepared for microbiota interaction, and a 180 mg/mL stock solution in DMSO for cell culture experiments.

2.2. Phytochemical screening

The analysis of extracts (MFE and CFE) (10 mg/mL MeOH) and the metabolic experiment samples was conducted using a UHPLC-3000 RS system (Dionex, Leipzig, Germany) coupled with a DAD detector and a splitless connection to an AmaZon SL ion trap mass spectrometer equipped with an ESI interface (Bruker Daltonik GmbH, Bremen, Germany). UV spectra were captured within the wavelength range of 200–450 nm. The mass spectrometer parameters were set as follows: nebulizer pressure at 40 psi, drying gas flow rate at 9.0 L/min, nitrogen gas temperature at 300°C, and capillary voltage at 4.5 kV. Mass spectra were recorded by scanning in the m/z range of 70 to 2200. A Kinetex XB-C18 chromatography column (Phenomenex, Torrance, CA; 150 mm × 2.1 mm; 1.7 µm) was employed. The mobile phase (A) consisted of UPW: HCOOH (99.9:0.1, *v*/*v*), while the mobile phase (B) was MeCN: HCOOH (99.9:0.1, *v*/*v*). The gradient program was set to 1–26% B over 0–60 min (0.416% B/min) and 26–95% B over 60–120 min (1.15% B/min) with a 0.3 mL/min flow rate. An injection volume of 4.0 µL (40 µg/µL) was used for all samples filtered through a 0.45 µm PVDF syringe filter.

2.3. Ex vivo experiments on skin microbiota

Skin microbiota were obtained from the forearms of five healthy volunteers by swabbing each forearm 10 times. Participants were instructed to refrain from showering on the day of sampling and to avoid applying any medications or cosmetic products to the forearm for at least 24h beforehand. The study was conducted in accordance with the Declaration of Helsinki and followed the guidelines of the Ethics Committee of the Medical University of Warsaw (AKBE/151/2021), which approved the collection of skin microbiota for *ex vivo* investigations.

After 24 h of microbiota pre-incubation, 1 mL of the extract was added to 5 mL of each donor sample to reach a final concentration of 2 mg/mL in the culture. Before use, the extract was sterilized by filtration through a 0.22 µm cellulose acetate syringe filter. Two types of controls were prepared: culture medium supplemented with the extract but without microbiota, and a method blank, in which donor microbiota were incubated without the extract. For the control with extract, 1 mL of the extract was added to 5 mL of BHI medium, whereas for the method blank, 1 mL of sterile water was added to 5 mL of the donor sample. All cultures were incubated at 37 °C with shaking at 120-140 rpm to ensure aeration (mini Galaxy A, RS Biotech, Nunc GmbH & Co, Wiesbaden, Germany).

2.3.1. Skin microbiota metabolism of the extract

At three timepoints (24, 48, and 72 h), 0.5 mL aliquots of each culture were collected from the microbiota culture, mixed with 0.5 mL of MeOH containing 0.2% HCOOH (1:1, *v*/*v*), and centrifuged at 10,000 rpm for 3 minutes to separate the microbial pellets. Supernatants were then subjected to UHPLC-DAD-MS^n analysis to evaluate changes in extract composition.

2.3.2. Skin microbiota sequencing

Amplification and sequencing of the 16S rDNA, accompanied by bioinformatic analysis, were conducted on the experimental samples following 24 hours of incubation with the addition of the studied extract. Samples from each donor were individually acquired utilizing the OmniGene-Skin kit. DNA extraction was conducted, followed by amplicon sequencing utilizing a two-stage PCR protocol and an Illumina sequencer. The V3–V4 region of 16S rDNA (341F-785R) was targeted with a universal primer set, producing 2.4 million paired-end sequence reads. The mean length of the aggregated sequences was 409 nucleotides. Chimeric reads were identified and removed using the UCHIME de novo algorithm [18] with the VSEARCH package [19]. The residual high-quality readings were subjected to minimum entropy decomposition [20]. To assign taxonomic information to each OTU, sequences from the clusters were aligned to the Mega BLAST database (https://blast.ncbi.nlm.nih.gov/). The QIIME program (version 1.9.1) was used for OTU processing and taxonomy classification. Abundances were normalized based on lineage-specific copy numbers of the relevant marker genes for more accurate estimates. Alpha diversity indices were calculated following the methods by Chao and Chiu from 2014 [21] and Thukral from 2017 [22]. Box plots were made using the ggplot2 and ggtext programs in R.

2.4. Keratinocytes and fibroblasts cell cultures

HaCaT and NHDF cells were obtained from Lonza Group Ltd. (Basel, Switzerland). DMEM High glucose w/stable glutamine w/sodium pyruvate, Dulbecco's Phosphate Buffered Saline (DPBS) without Ca^{2+} and Mg^{2+}, fetal bovine serum (FBS), penicillin-streptomycin solution, Trypsin-EDTA solution were purchased from Biowest (Nuaille, France). Interferon-γ and TNF-α were obtained from InvivoGen (Toulouse, France), lipoteichoic acid (LTA) from *Staphylococcus aureus*, and dimethylsulfoxide (DMSO) from Sigma Aldrich (United States). IL-6 and IL-8 ELISA kits were from BD Bioscience (San Diego, USA).

Cells were cultured in high-glucose DMEM supplemented with 10% FBS and antibiotics (penicillin and streptomycin). The medium was replaced every 2–3 days using standard aseptic procedures. Cells from flasks that were 70–90% confluent and had over 90% viability were then seeded into 96-well or 24-well culture plates at the specified densities

2.5. Keratinocytes and fibroblasts viability evaluation

HaCaT (7×10^3) and NHDF (5×10^3) cells were seeded into 96-well plates and allowed to grow until reaching 90% confluency. Following this, the cells were treated with previously prepared dilutions of the extracts, 7.8 – 1000 µg/mL, and incubated for 72 hours. Cell fixation was then performed by adding 50 µL/well of 50% trichloroacetic acid (TCA). After a 1-hour incubation at 4°C, the plates were rinsed with water and air-dried. Subsequently, the cell monolayer was stained with 0.04% Sulforhodamine B (SRB) sodium salt. After a 1-hour incubation, the plates were washed with 1% acetic acid

and dried. Finally, 10 mM Tris base was added to solubilize the protein-bound dye, and absorbance was measured at 510 nm.

2.6. Evaluation of IL-6 and IL-8 secretion

To quantify cytokines' release, HaCaT (4×10^4) and NHDF (7×10^4) were seeded into 24-well plates. Once the cultures reached approximately 90% confluence, they were treated with marigold extract at 7.8 – 250 µg/mL concentrations and chamomile extract at 15.6 – 500 µg/mL concentrations. For NHDF, the stimulus (LTA) was added simultaneously with the treatment, whereas for HaCat, the stimuli (mixture of TNF-α and IFN-γ) were added 3h after treatment. After 24h, 200 µL of the supernatant from each well was collected from three independent experiments and stored at − 20 °C until analysis. Interleukin concentrations were measured by an enzyme-linked immunosorbent assay (ELISA) using a commercially available human IL-6 and IL-8 kits (BD Bioscience, USA), following the manufacturer's protocols. Absorbance was measured at 450 nm with correction at 570 nm using a Synergy 4 microplate reader (Biotek).

2.7. Statistical analysis

The results were presented as means ± standard deviation of the means. Statistical significance of differences between means was determined by one-way ANOVA. For comparison of results with the control group, Dunnett's post hoc test was used. Results with *p-value* < 0.05 and *p-value* < 0.001 were considered statistically significant. All analyses were performed using Statistica 10 software.

3. Results and discussion

3.1. Chemical extracts' constituents assessment

The hydroethanolic flower extracts of marigold flowers (MFE) and chamomile flowers (CFE) were subjected to UHPLC-DAD-MS^n analysis, through which a method for assessing their chemical composition was established (**Fig. 1, Table 1**, and **Fig. 2, Table 2** accordingly).

3.1.1. Phytochemical screening of marigold flower extract (MFE)

Peak **1** exhibited a $[M\text{-}H]^-$ ion at 353 *m/z*, identified as chlorogenic acid, with a primary fragment at 191 *m/z* due to the loss of a quinic acid moiety. In the positive mode, a 355 *m/z* ion was observed, further fragmenting into 336, 307, and 163 *m/z* ions [23]. Peak **2** produced a $[M\text{-}H]^+$ ion at 415 *m/z*, corresponding to an undefined compound, with fragmentation resulting in ions at 219 *m/z*. Peak **3** showed a $[M\text{-}H]^-$ ion at 755 *m/z*, representing quercetin-3-O-(2″,6″-di-O-rhamnosyl)-glucopyranoside, with fragments at 737, 609, 591, 573, 547, 489, 465, 409, 343, 300, 271, and 255 *m/z*. It was isolated and identified by Weronika Skowrońska [24]. Peak **4** produced a $[M\text{-}H]^-$ ion at 609 *m/z*, identified as calendoflavobioside, which fragmented into 489, 463, 445, 343, 301, 300, 271, and 179*m/z* ions [23]. The positive mode detected a 611 m/z ion, with further fragmentation into 465, 303, and 315 *m/z* ions. Peak **5** had an $[M\text{-}H]^-$ ion at 769 *m/z*, identified as isorhamnetin-3-*O*-rhamnosylrutinoside, with fragmentation leading to ions at 423, 369, 357, 315, 314, and 300 *m/z* [25]. The positive mode detected at 771 *m/z* revealed additional fragments at 625, 479, 427, and 317 *m/z*. Peak **6** produced a $[M\text{-}H]^-$ ion at 623 *m/z*, corresponding to isorhamnetin-3-*O*-rutinoside, which fragmented into 605, 503, 357, 339, 315, and 299 *m/z* ions [25]. Peak **7** displayed a $[M\text{-}H]^-$ ion at 623 *m/z*, identified as calendoflavoside, with a fragmentation pattern yielding ions at 591, 503, 477, 459, 383, 356, 314b, and 299 *m/z*. In the positive mode, prominent fragments were detected at 479 and 317 *m/z* [23]. Peak **8** showed a $[M\text{-}H]^-$ ion at 609 *m/z*, corresponding to rutin, with fragments at 577, 477, 459, and $[M\text{-}H]^+$ at 611 *m/z*, and further fragmentation into 479 and 317 *m/z* ions in the positive mode [23]. Peak **9** displayed a $[M\text{-}H]^-$ ion at 623 *m/z*, corresponding to narcisin, with fragments at 315, 299, 271, and 255 *m/z*. In the positive mode, a 625 *m/z* ion was observed, which further fragmented into 479 and 317 *m/z* ions [23]. Peak **10**, assigned to isorhamnetin-3-*O*-glucoside, showed a $[M\text{-}H]^-$ ion at 477 *m/z*, yielding fragments at 357, 314, and 285 *m/z*. The positive mode revealed a primary ion at 479 *m/z*, alongside 302 and 165 *m/z* fragments [26]. Peak **11**, linked to isorhamnetin-3-*O*-(6″-acetyl)-glucoside, generated a $[M\text{-}H]^-$ ion at 519 *m/z*, fragmenting into 315 and 300 *m/z* ions, while the $[M\text{-}H]^+$ detected a 565 *m/z* ion [26]. Peak **12**, an unidentified compound, exhibited a $[M\text{-}H]^-$ ion at 589 *m/z*, with fragmentation producing 584 and 485 *m/z* ions. Peak **13**, identified as oleanolic acid glucuronide A, showed a $[M\text{-}H]^-$ ion at 1118 *m/z*, with fragments at 955, 793, 549, and 455 *m/z*, and a $[M\text{-}H]^+$ ion at 439 with fragmentations at 393, 329, 249, and 191 *m/z* [25]. Peak **14**, corresponding to oleanolic acid glucuronide C, displayed a $[M\text{-}H]^-$ ion at 956 *m/z*, with fragmentation resulting in 794, 483 *m/z* ions [25]. Peak **15**, linked to oleanolic acid glucuronide B, produced a $[M\text{-}H]^-$ ion at 793 *m/z*, fragmenting into ions at 673, 631, and 569 *m/z* [25]. Peak **16**, associated with oleanolic acid glucuronide C, showed a $[M\text{-}H]^-$ ion at 955 *m/z*, with fragments at 793, 776, and 713 *m/z*. Peak **17**, representing oleanolic acid glucuronide D, exhibited a $[M\text{-}H]^-$ ion at 793 *m/z*, with fragmentation yielding 731, 613, 595, 569, 551, 537, 483, and 455*m/z* ions [25]. Peak **18**, identified as oleanolic acid glucuronide E, showed a $[M\text{-}H]^-$ ion at 631 *m/z*, fragmenting into 613, 571, 555, 527, 509, and 455 *m/z* ions [25].

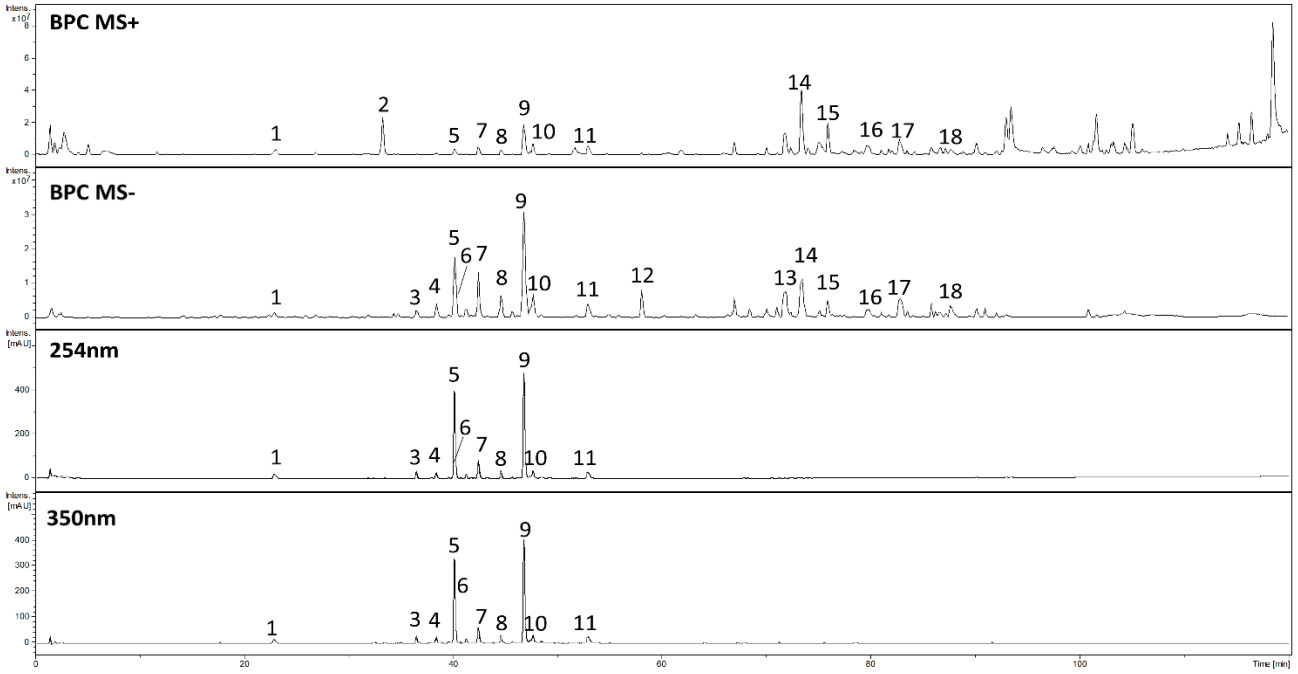

Fig 1. UHPLC-DAD-MS data of the 70% ethanolic extract of marigold flowers (MFE) were recorded in the mode of positive ions (MS+), negative ions (MS-), and UV of 254 and 350 nm.

Table 1. UHPLC-DAD-MS data of detected compounds in the 70% ethanolic extract from the marigold flowers (MFE).

Peak number	Retention time [min]	UV-Vis max [nm]	$[M-H]^-$ *m/z*	MS2 ions (-)	MS3 ions (-)	$[M-H]^+$ *m/z*	MS2 ions (+)	MS3 ions (+)	Compound name	Ref.
1	23.1	248sh, 334	353	191	-	355	336, 307, 163b	-	chlorogenic acid	[23]
2	33.3	-	-	-	-	415	219b	-	unidentified compound	-
3	36.5	254, 265sh, 356	755	737, 609, 591, 573, 547, 489, 465, 409, 343, 300b, 271,255	531, 445, 400, 383, 373, 355, 343b, 313, 301, 297, 271, 267, 254	-	-	-	quercetin-3-*O*-(2″,6″-di-*O*-rhamnosyl)-glucopyranoside	[24]
4	38.4	254, 356	609	489, 463, 445, 343, 301, 300b, 271, 179	373, 343, 301b	611	465, 303b	447, 399, 315, 303b	calendoflavobioside	[23]
5	40.2	253, 265sh, 355	769	737, 624, 605, 503, 423, 369, 357, 315, 314, 300	-	771	625, 479, 427, 317b, 229	-	isorhamnetin-3-*O*-rhamnosylrutinoside	[25]
6	40.2	253, 265sh, 355	623	605, 503, 357, 339, 315b, 299	-	-	-	-	isorhamnetin-3-*O*-rutinoside	[26]
7	42.5	253, 265sh, 354	623	591, 503, 477, 459, 383, 356, 314b, 299	-	625	479, 317b	461, 425, 383, 359, 329, 317b	calendoflavoside	[23]
8	44.7	253, 267sh, 354	609	577, 477, 459, 339, 315b, 271, 179	-	611	479, 317b	-	rutin	[23]
9	46.8	253, 267sh, 354	623	315b, 299, 271, 255	-	625	479, 317b	-	narcissin	[23]
10	47.8	253, 264, 341	477	357, 314b, 285, 271, 151	-	479	302, 165b, 163	-	isorhamnetin-3-*O*-glucoside	[26]
11	53.0	253, 265, 354	519	315b, 300	-	565[c]	317b	-	isorhamnetin-3-*O*-(6″-acetyl)-glucoside	[23]
12	58.1	-	589	584b, 485	-	-	-		unidentified compound	-
13	71.8	-	1118[d+ac]	955b, 793, 549, 455	793b, 569, 549, 455	439	393, 329, 249, 191	-	oleanolic acid glucuronide A	[25]
14	73.5	-	956	794b, 483	614, 595, 551, 537 485, 484 483b, 455	-	-	-	oleanolic acid glucuronide C	[25]
15	75.9	-	793[d+s]	673, 631b, 569	555, 509, 455b	-	-	-	oleanolic acid glucuronide	
16	79.8	-	955	793, 776, 731, 713, 613, 595, 569, 551, 538, 524, 455b	631, 614, 613, 595, 587, 569, 537, 524, 523b, 483, 455, 453	-	-	-	oleanolic acid glucuronide B	[25]
17	82.8	-	793	731, 613, 595, 569, 551, 537, 483, 455	-	-	-	-	oleanolic acid glucuronide D	[25]
18	87.7	-	631	613, 571, 555, 527, 509, 455b	407b	-	-	-	oleanolic acid glucuronide F	[25]

b – base peak (the most abundant ion in the recorded spectrum); sh – shoulder in UV-Vis spectrum; [ac] – acetyl unit $[M+42]^-$; [c] – carboxyl unit $[M+44]^-$; [d] – double mass; [s] – sodium $[M+Na]^-$.

3.1.2. Phytochemical screening of chamomile flower extract (CFE)

Peaks **19** and **20** gave $[M\text{-}H]^-$ ions of 355 *m/z*. These were identified as 2-hydroxy-4-methoxyoxycinnamic acid glucoside [27]. They fragmented into a 193 *m/z* peak, during which the hexose was lost, and a 149 *m/z* peak formed by the detachment of an additional CO_2 molecule (-44), indicating that the carboxylic acid in the cinnamic group was free, unesterified. Further loss of the methyl group was observed for peak **19** at 134 *m/z* and was typical of homolytic cleavage of the methyl belonging to the methoxyl group. The differentiation of peak **19** into cis-2-hydroxy-4-methoxy-coccinnamic acid glucoside and peak **20** into trans-2-hydroxy-4-methoxy-coccinnamic acid glucoside was made possible by the occurrence of an additional peak in UV-Vis at 320 nm, being characteristic of the cis isomer [27]. Peak **21** gave a $[M\text{-}H]^-$ ion of 479 *m/z*, which indicates the presence of quercetagenin 3-*O*-glucoside. It decayed into a peak with a mass of 317 *m/z*, probably by loss of glucose [28]. Peaks **22** and **23** gave ions $[M\text{-}H]^-$ with masses of 463 *m/z* derived from hyperoside and isoquercetin. These compounds have the same masses, but hyperoside has a lower retention time than isoquercetin [29]. Peak **24** was identified as luteolin hexoside with $[M\text{-}H]^-$ ion at 447 *m/z*, and $[M\text{-}H]^+$ ion at 449 *m/z*, while peak **25** was identified as patuletin 3-*O*-glucoside, as it is derived from the $[M\text{-}H]^-$ ion of 493 *m/z*. Peak **26** shows a signal from the $[M\text{-}H]^-$ ion with a mass of 493 *m/z*. An absorption maximum was observed at 355 nm, so it is known that the sugar group is in position 3, causing a hypochromic shift relative to the aglycone itself. On this basis, the compound was identified as apigenin-7-*O*-glucoside [27]. In the case of luteolin-7-*O*-glucoside (**27**) and chrysoeriol 7-*O*-glicoside (**28**), the addition of one additional oxygen substitution on C-3′ results in a bathochromic shift of band I at ~ 347 nm, while band II shows a cleavage of its peak, giving rise to a characteristic arm at 267 nm. Compound **29** was recognized as quercetin-7-*O*-glucoside additionally due to the information of its $[M\text{-}H]^-$ peak mass of 507 *m/z* [27]. Peak **30** arose from the $[M\text{-}H]^-$ ion with a mass of 515 *m/z*, indicating that it is dicaffeoylquinic acid derivative [27]. Peak **31** and **32** with an $[M\text{-}H]^-$ mass of 517 *m/z* were identified as isorhamnetin-7-*O*-glucoside and isorhamnetin-3-*O*-glucoside, accordingly [27,29]. Peak **33** showed a signal from the [M-H]+ ion with a mass of 269 *m/z*, and although the chromatogram did not show fragmentation of this ion, due to the signal intensity being too weak, it was identified as apigenin [28]. Peak **34** was recognized as 3-hydroxydecanoic acid, with an $[M\text{-}H]^-$ mass of 373 *m/z* and $[M\text{-}H]^+$ mass of 375 *m/z* [30]. Peak **35** is from the [M-H]- ion with a mass of 373 *m/z*. It shows absorption maxima at 319 nm and 341 nm. Based on this, the compound was identified as dihydroxytetramethoxyflavone [28]. Peaks **36-40** could not be identified from the available literature.

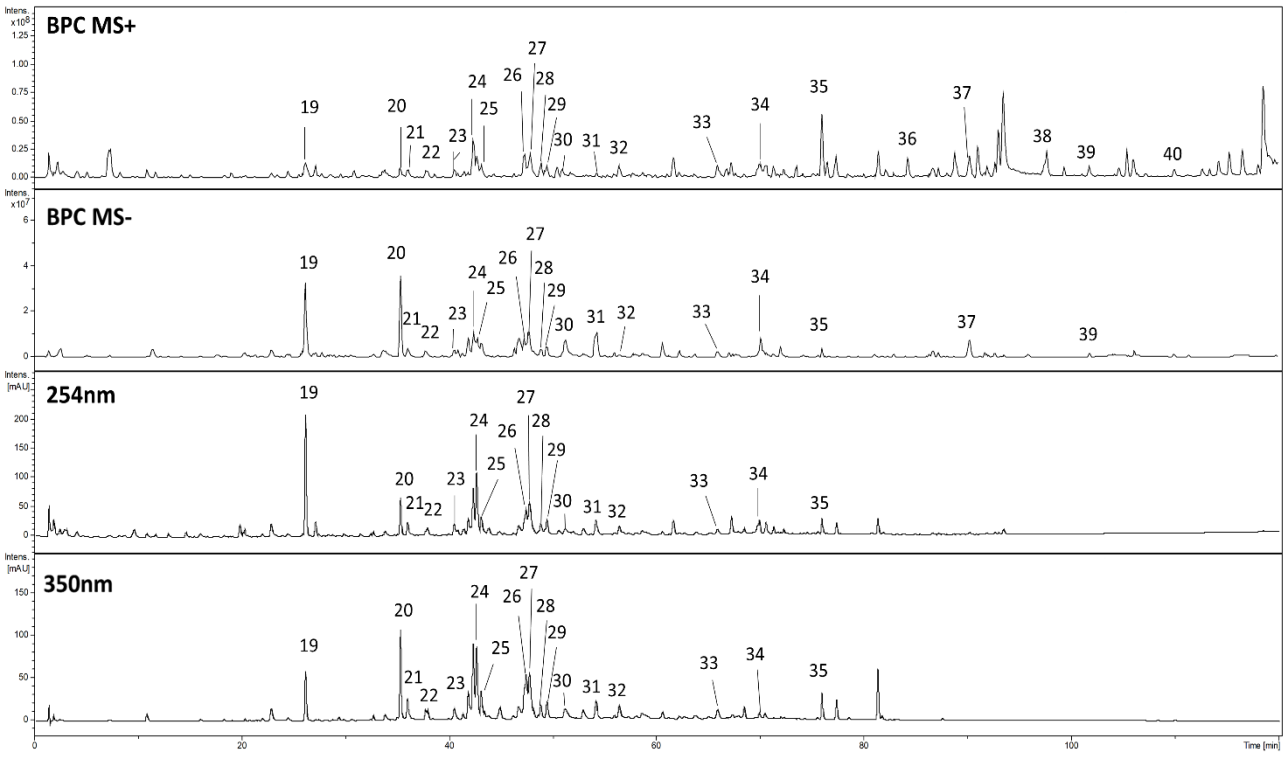

Fig 2. UHPLC-DAD-MS data of the 70% ethanolic extract of chamomile flowers (CFE) were recorded in the mode of positive ions (MS+), negative ions (MS-), and UV of 254 and 350 nm.

Table 2. UHPLC-DAD-MS data of detected compounds in the 70% ethanolic extract from the chamomile flowers (CFE).

Peak number	Retention time [min]	UV-Vis max [nm]	[M-H]- *m/z*	MS2 (-)	[M-H]+ *m/z*	MS2 (+)	Compound name	Ref.
19	26.10	280, 301sh	355	193b, 149, 134	379c	365b, 203, 185, 173	cis-2-hydroxy-4-methoxyoxocinnamic acid glucoside	[27]
20	35.20	287, 320	355	193b, 149	379c	361, 292, 202, 154	trans-2-hydroxy-4-methoxycinnamic acid glucoside	[27]
21	35.90	258, 276, 352	479	317b	481	319b	quercetagenin-3-*O*-glucoside	[27]
22	37.60	278, 377	463	301b	465	421, 303b	quercetin-3-*O*-galactoside (hyperoside)	[29]
23	40.40	253, 368	463	301b, 343	465	303b	quercetin-3-*O*-glucoside (isoquercetin)	[29]
24	42.60	257, 368	447	285b, 286	449	287b, 288	luteolin hexoside	[29]
25	43.00	257, 275, 355	493	331b	495	333b	patuletin 3-*O*-glucoside	[27]
26	47.30	252h, 268, 328	431	269b	433	271b	apigenin 7-*O*-glucoside	[27]
27	47.70	267, 285, 337	447	285b	449	287b	luteolin-7-*O*-glucoside (cynaroside)	[28]
28	48.80	267, 289, 346	461	299b, 446, 284	463	301b, 302	chrysoeriol-7-*O*-glucoside	[27]
29	49.40	257, 272, 364	507[fa]	387, 345b	463	347b	quercetin-7-*O*-glucoside	[27]
30	51.30	300, 330	515	353b, 203	517	353b, 299, 255, 203, 179, 173	dicaffeoylquinic acid derivative	[27]
31	54.10	295sh, 325	517	323b, 281, 179, 251, 355, 193, 2210, 341, 437, 353	541[c]	365, 347b	isorhamnetin-7-*O*-glucoside	[27]
32	56.30	265, 340	517	473, 269b, 268	519	433, 271b	isorhamnetin-3-*O*-glucoside	[27,29]
33	65.80	269, 337	269	-	271	-	apigenin	[28]
34	70.10	350	329	293, 264, 229b, 211, 171	353[c]	-	3-hydroxydecanoic acid	[30]
35	75.90	319, 341sh	373	358b, 359	375	356,342, 311b	dihydroxytetramethoxyflavone	[28]
36	84.30	-	-	-	499	261b	unidentified compound	-
37	90.30	-	295	277b, 233, 170	319[c]	277b, 233, 171,	unidentified compound	-
38	97.70	-	-	-	341	-	unidentified compound	-
39	101.80	-	277	233b	279	261, 243, 223, 205b,	unidentified compound	-
40	110.10	-	-	-	593	533b, 461	unidentified compound	-

b – base peak (the most abundant ion in the recorded spectrum); sh – shoulder in UV-Vis spectrum; [c] - carboxyl unit $[M+44]^-$; [fa] – formic acid $[M+46]^-$.

3.2. *Ex vivo* skin microbiota metabolism of the extract

The hydroethanolic extracts of *Calendulae officinalis* flos and *Matricariae recutita flos* were incubated with skin microbiota for 24 h to assess possible biotransformation processes. Previous studies on microbiota showed that under microbiota influence, secondary metabolites from the extract can be generated, which enhance biological activity [14]. Moreover, our previous study on comfrey root showed that the chemical composition of the extract was biodegraded by skin microbiota [31]. In the case of marigold and chamomile flowers, UHPLC-DAD-MSn analysis revealed that the chemical profile of the extracts remained unchanged after incubation (**Fig. 3-4**).

In both extracts, no new metabolites were detected, and all initially identified constituents of the extracts retained their stability throughout the experiment. This may reflect the relative stability of the main phytochemical constituents, such as flavonoids and terpenoids, which are less prone to microbial transformation compared to glycoside-rich or alkaloid-containing plants. These findings indicate that, under the applied conditions, the skin microbiota did not induce any metabolic conversion of the extracts' components. Importantly, such stability can be considered a favorable outcome, as it suggests that the tested phytochemicals are resistant to microbial transformation within the studied model, which may support their persistence and activity when applied topically.

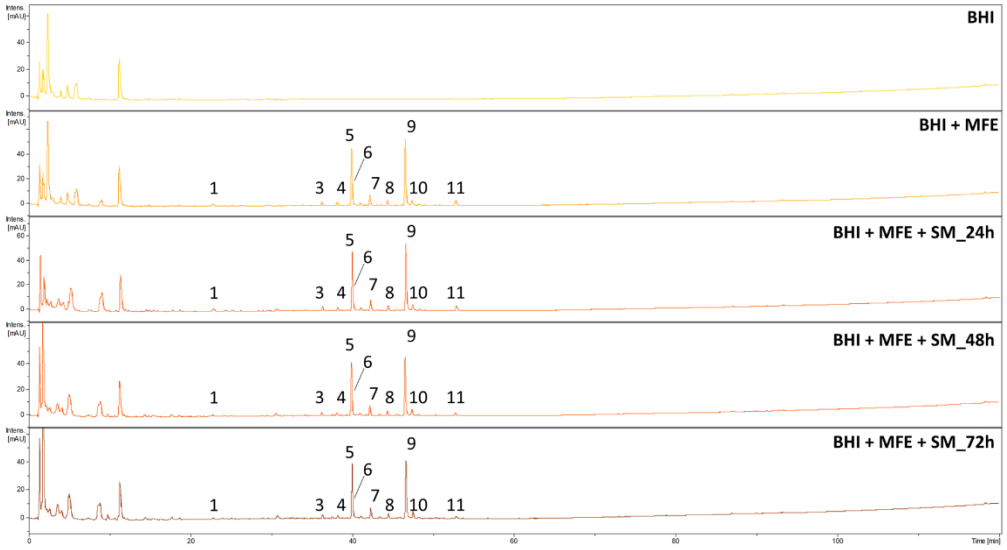

Fig. 3. UHPLC-DAD-MSn chromatograms in the UV of 254 nm of *Calendula officinalis* extract after 24, 48, 72 h incubation with human skin microbiota, showing no detectable metabolite formation, confirming chemical stability of MFE under microbiota influence. BHI, brain heart infusion; MFE, marigold flower extract; SM, skin microbiota.

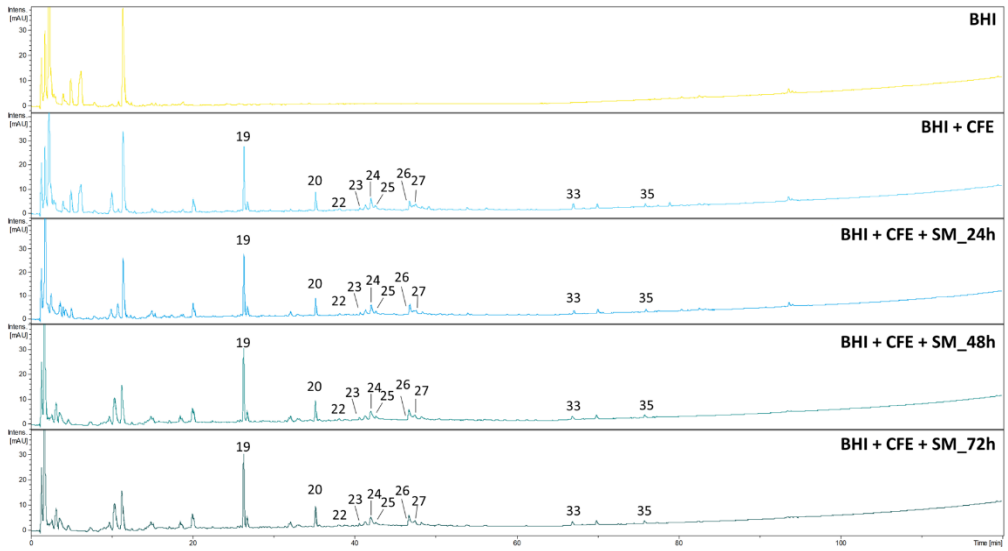

Fig. 4. UHPLC-DAD-MSn chromatograms in the UV of 254 nm of *Matricaria recutita* extract after 24, 48, 72 h incubation with human skin microbiota, showing no detectable metabolite formation, confirming chemical stability of CFE under microbiota influence. BHI, brain heart infusion; CFE, chamomile flower extract; SM, skin microbiota.

3.3. Skin microbiota modulation by MFE and CGE

In a comparative analysis of skin microbiota profiles between untreated controls and samples incubated with plant extracts for 24 h, reproducible shifts in the relative composition of the community were found. Control samples reflect the baseline community structure with the expected dominance of several taxa and the contribution of low-abundant groups.

In the experiment involving *C. officinalis* extract (**Fig. 5**), the microbiota community was dominated by members of the families *Staphylococcaceae*, *Bacillaceae*, *Enterococcaceae*, and unclassified *Bacillales*. After exposure to the extract, a redistribution of the shares of dominant and subdominant taxa is observed. The relative abundance of *Staphylococcaceae*, *Corynebacteriaceae*, *Enterococcaceae*, *Lactobacillaceae, and Leuconostocaceae* decreased, whereas unclassified *Bacillales* relatively increased.

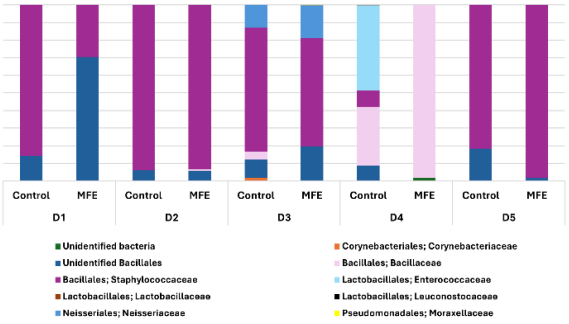

Fig.5. The relative order and family abundance in samples after 24 h incubation. MFE, marigold flower extract; D1-5, donor number.

Notably, several bacterial families (e.g., unclassified *Bacteria* and *Moraxellaceae*) were absent in the control profile, but appeared after 24 h incubation with the extract. This likely reflects taxa that were initially present at very low abundance and became detectable after selective suppression of dominant orders. Such emergence can be interpreted as the result of ecological niche and/or selective stimulation by extract components, rather than true *de novo* colonization. Also, it can be because of the detection effect of sequencing, as taxa could be present in the control in extremely low numbers (below the detection threshold or statistically "masked" by dominant taxa). The presence of extract constituents alters the culture environment, enabling those taxa to increase their abundance above the noise level.

It indicates that the extracts selectively suppressed some taxa while allowing some groups to expand. This suggests a modulatory rather than broad-spectrum antimicrobial effect, leading to a rebalancing of the skin microbial community. Additionally, the maintenance of α-diversity indicates that the extract does not exhibit broad-spectrum antimicrobial activity, although treatment with *C. officinalis* influenced microbial community structure (**Fig. 6**). The Chao-1 index (**Fig. 6, A**) revealed a tendency towards lower richness in the MFE group compared to the control, indicating a reduction in the number of observed taxa. The Shannon (**Fig. 6, B**) and Simpson (**Fig. 6, C**) indices also demonstrated a more uniform distribution in MFE-treated samples, with slightly lower median values relative to the control.

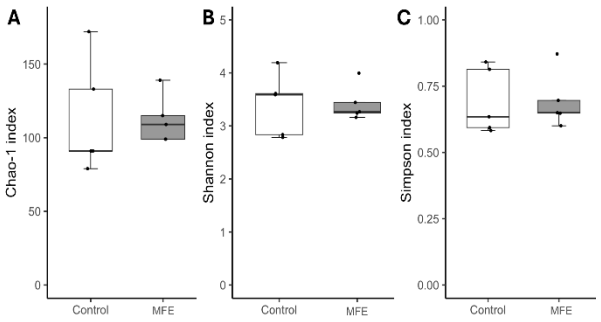

Fig. 6. Boxplots of α-diversity: Chao 1 (A), Shannon (B), Simpson (C) indices. MFE, marigold flower extract.

During the evaluation of *M. recutita* extract, the skin microbiota was primarily composed of the unclassified *Bacillales*, *Staphylococcaceae*, and one donor had *Bacillaceae* (**Fig. 7**). Exposure to the extract resulted in the redistribution of dominant and subdominant taxa as well. A reduction in the relative abundance of unclassified bacteria and *Pseudomonadaceae* was noted, while *Bacillaceae* increased. The response of other bacterial groups varied among donors.

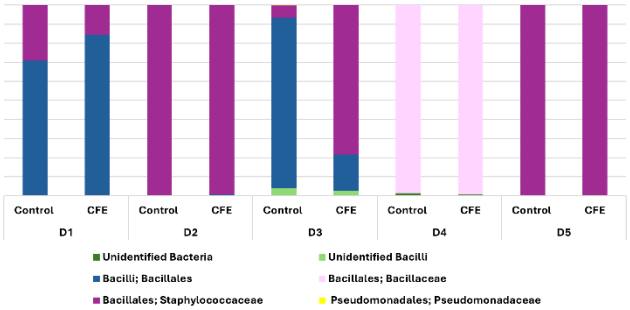

Fig. 7. The relative order and family abundance in samples after 24 h incubation. CFE, Chamomilla flower extract; D1-5, donor number.

Analysis of α-diversity revealed that exposure to chamomile flower extract affected microbial community richness and diversity (**Fig. 8**). The Chao-1 richness (**Fig. 8, A**) showed a broader distribution of values in the CFE group compared with the control, suggesting donor-dependent changes in the number of observed taxa. Similarly, the Shannon (**Fig. 8, B**) and Simpson (**Fig. 8, C**) indices indicated increased variability after CFE treatment, with some samples showing higher diversity than the control group. These results suggest the CFE modulates microbial diversity in a heterogeneous manner, reflecting interindividual differences in microbiota response.

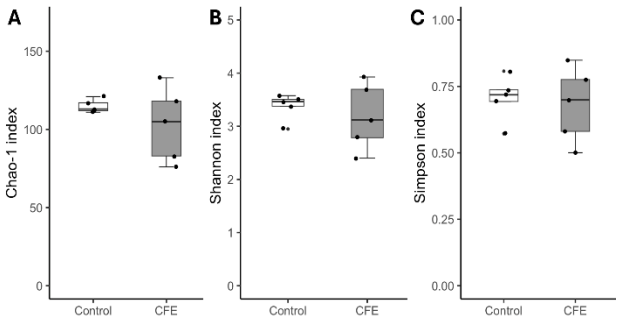

Fig. 8. Boxplots of α-diversity: Chao 1 (A), Shannon (B), Simpson (C) indices. CFE, Chamomilla flower extract

Comparison of the effects of marigold and chamomilla flower extracts on the skin microbiota revealed distinct patterns of modulation. CFE increased inter-donor variability, with some samples showing higher richness and diversity compared with the control. This suggests a more selective and individualized influence on microbial communities, potentially stimulating certain beneficial taxa while suppressing others. In contrast, MFE led to an overall reduction in richness and diversity indices, accompanied by decreased variability between donors. Such an effect indicated a broader and uniform impact on microbial populations, which may reflect a stronger antimicrobial or growth-limiting action. Taken together, these findings highlight that although both extracts modulate microbial communities, chamomile appears to promote donor-dependent diversification, whereas calendula exerts a more homogenizing effect by reducing overall community complexity. These differences may be attributed to their distinct phytochemical compositions, which could differentially influence microbial growth and interactions.

3.4. Keratinocytes and fibroblasts viability evaluation

Keratinocytes and fibroblasts viability was assessed using the colorimetric method, Sulforhodamine B assay, to determine cell viability and growth by quantifying total cellular protein content [32]. The assay is based on the binding of the anionic dye to basic amino acid residues of cellular proteins that remain attached to the culture plate after fixation. The amount of bound dye is directly proportional to the total protein mass and, consequently, to the number of viable cells.

Cell viability is expressed as a percentage of the absorbance of untreated control cells. The SRB assay offers a sensitive and reproducible method for evaluating the impact of plant extracts, drugs, or other agents on cell proliferation and cytotoxicity [33].

3.4.1. Viability of HaCaT keratinocytes

Treatment of keratinocytes with marigold flower extract revealed a pronounced dose-dependent biphasic effect on cell viability (**Fig. 9, A**). At high concentrations (1000 and 500 µg/mL), a significant reduction in metabolic activity was observed ($p < 0.001$), indicating potential cytotoxic or growth-inhibitory effects of the concentrated extracts. Such reduction may be associated with the presence of saponins, flavonoids, or other phenolic constituents known for their membrane-active or pro-oxidant behavior at elevated doses [34]. In contrast, moderate to low concentrations (250-7.8 µg/mL) did not impair HaCaT viability, and in fact, at 125-31.3 µg/mL, the extract markedly stimulated cell proliferation, reaching approximately 107-110% of the control value ($p < 0.05$; $p < 0.001$). This stimulatory response suggests a potential adaptive effect, where sub-cytotoxic doses enhance metabolic and proliferative activity, possibly due to activation of antioxidant defense mechanisms or modulation of growth factor signaling pathways.

Exposure of HaCaT to chamomile flower extract resulted in a mild concentration-dependent response with no marked cytotoxicity across most tested doses (**Fig. 9, B**). Only the highest concentration (1000 µg/mL) significantly reduced cell viability ($p < 0.001$), indicating that excessive amounts of the extract may exert mild cytostatic or membrane-perturbing effects.

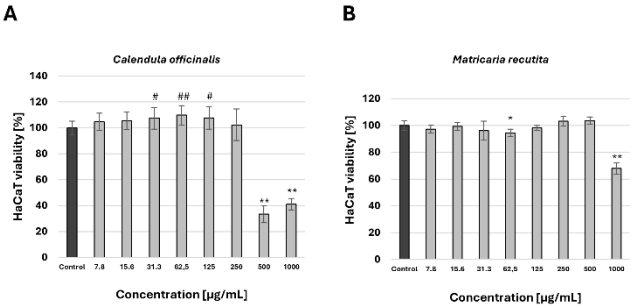

Fig.9. The viability of HaCaT cells assessed after 24 h of treatment with extract of *Calendula officinalis* (A) and *Matricaria recutita* (B) (SRB assay). A statistically significant increase (#$p < 0.05$; ##$p < 0.001$) or decrease (*$p < 0.05$; **$p < 0.001$) was indicated relative to control.

Such outcomes at high doses are consistent with the presence of sesquiterpene lactones and phenolic acids, which may induce oxidative stress or alter mitochondrial function when accumulated intracellularly [35]. At lowest concentrations, 250 – 7.8 µg/mL, no notable proliferative effect was detected, indicating that CFE primarily stabilizes cellular metabolism rather than directly stimulating proliferation. This neutral or protective action might reflect a predominance of phenolic acids and flavonoids with anti-inflammatory and antioxidant activity, which help preserve keratinocytes' homeostasis without overactivation.

Both extracts exhibited dose-dependent cytotoxicity at the highest concentrations, while maintaining good biocompatibility at ≤ 250 and 500 µg/mL, respectively. These findings confirm that both extracts are safe and non-cytotoxic for epidermal application at moderate concentrations.

3.4.2. Viability of NHDF fibroblasts

The viability of NHDF after exposure to extracts of *Calendula officinalis* and *Matricaria recutita* demonstrated distinct but concentration-dependent trends (**Fig. 10**).

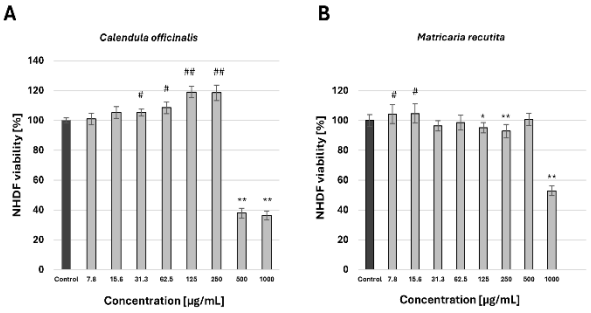

Fig.10. The viability of NHDF cells assessed after 72 h of treatment with extract of *Calendula officinalis* (A) and *Matricaria recutita* (B) (SRB assay). A statistically significant increase (#$p < 0.05$; ##$p < 0.001$) or decrease (*$p < 0.05$; **$p < 0.001$) was indicated relative to the control.

In the case of marigold (**Fig. 10, A**), fibroblasts responded in a biphasic manner. At low and moderate concentrations (7.8 - 250 µg/mL), a slight but consistent increase in viability was observed, with a maximum of

approximately 120% compared to the control at 125-250 µg/mL. This suggests that MFE at sub-cytotoxic levels may stimulate fibroblasts' metabolic activity and proliferation. Such effects are typical for phytochemicals with antioxidant and trophic properties, which can promote dermal repair and collagen synthesis. However, at 500-1000 µg/mL, cell viability dropped below 40%, indicating cytotoxicity likely associated with excessive accumulation of bioactive compounds.

CFE (**Fig. 10, B**) maintained fibroblast viability near the control level across most concentrations, demonstrating good cytocompatibility and absence of toxic effects. A moderate decrease was observed only at the higher concentrations (1000 µg/mL), similar to MFE, suggesting a threshold-dependent response. Unlike MFE, no notable proliferative effect was detected, indicating that CFE primarily stabilizes cellular metabolism rather than directly stimulating proliferation. Just at low concentrations, 15.6 – 7.8 µg/mL, the extract maintained slightly increased cell viability compared to the control, with values remaining 105% of baseline. This suggests that *Matricaria recutita* is well tolerated by NHDF cells and can support cell survival even under prolonged exposure. The observed biocompatibility aligns with its traditional dermatological applications and reported antioxidant, anti-inflammatory, and soothing effects.

Overall, both extracts were well tolerated by NHDF cells at concentrations ≤ 250 and 500 µg/mL, respectively. The biphasic pattern observed for MFE supports the hypothesis that plant-derived antioxidants may exhibit dose-dependent duality – protective at low doses and cytotoxic when overloaded. These findings highlight the potential of both extracts as safe and biologically active components for dermal applications.

3.5. Anti-inflammatory potential of extracts

Skin inflammation represents a complex, multi-stage biological response that involves both epidermal and dermal cell populations. It is initiated primarily by keratinocytes, which, upon exposure to pro-inflammatory cytokines such as tumor necrosis factor and interferons, release a wide range of mediators, including interleukin-6 and interleukin-8 [36]. These cytokines act as central regulators of the cutaneous immune response – IL-6 contributes to leukocyte activation, acute-phase protein synthesis, and modulation of keratinocyte proliferation, while IL-8 serves as a potent chemoattractant for neutrophils and macrophages, amplifying the inflammatory cascade [37,38]. Sustained overproduction of these mediators is associated with chronic inflammatory skin disorders such as atopic dermatitis, psoriasis, and delayed wound healing [38].

In the dermis, fibroblasts further sustain and propagate inflammation through cytokine secretion and paracrine crosstalk with immune cells and keratinocytes. Thus, simultaneous assessment of inflammatory markers in both HaCaT and NHDF provides an integrated model for evaluating the dual epidermal and dermal anti-inflammatory actions of bioactive compounds.

Plant extracts rich in polyphenols, triterpenoids, and glycosides have been shown to modulate inflammatory signaling pathways, including NF-κB, MAPK, and STAT1/3, thereby reducing cytokine production and oxidative stress [39–41]. In this study, the anti-inflammatory potential of the tested extracts from *Calendulae officinalis flos* and *Matricariae recutita flos* was investigated by measuring their ability to regulate IL-6 and IL-8 secretion in both types of skin cells.

3.5.1. Modulation of IL-6 and IL-8 secretion in HaCaT keratinocytes

HaCaT cells were stimulated with TNF-α/IFN-γ to induce cytokine production and to evaluate the potential of the tested extracts to modulate this response. Stimulation markedly increased the secretion of IL-6 and IL-8 compared with the non-stimulated control. Urolithin A was used as a positive control, reducing both IL-6 and IL-8 secretion in a dose-dependent manner.

Treatment with *Calendula officinalis* extract did not result in significant suppression of IL-6 secretion at any of the tested concentrations (7.8 – 250 µg/mL) (**Fig. 11**). Similarly, IL-8 release remained unchanged, with values close to those of the stimulated control (**Fig. 12**). These results suggest that, within the tested concentration range, *Calendula officinalis* exhibits a lack of pronounced anti-inflammatory efficacy in keratinocytes under TNF-α/IFN-γ challenge.

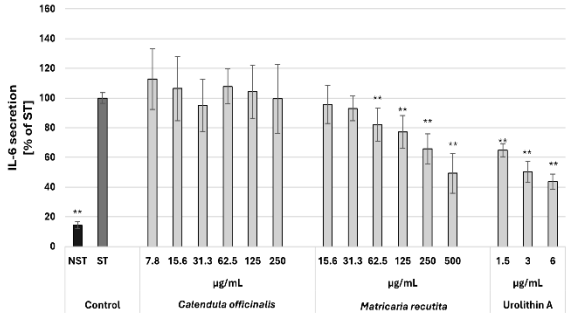

Fig.11. Effect on IL-6 release in HaCaT cells stimulated with a TNF-α/IFN-γ mixture (10 ng/mL each). A statistically significant increase (#p < 0.05; ##p <0.001) or decrease (*p < 0.05; **p < 0.001) was observed compared with stimulated control.

In contrast, *Matricaria recutita* extract demonstrated a distinct modulatory effect. A concentration-dependent decrease in IL-6 secretion was observed, with reductions of approximately 50-70% at concentrations of 250 and 500 µg/mL (*p < 0.05; **p < 0.001, respectively) **(Fig. 11).** The suppression of IL-8 secretion was less pronounced and did not consistently reach statistical significance, indicating a more selective action towards IL-6 modulation **(Fig. 12).**

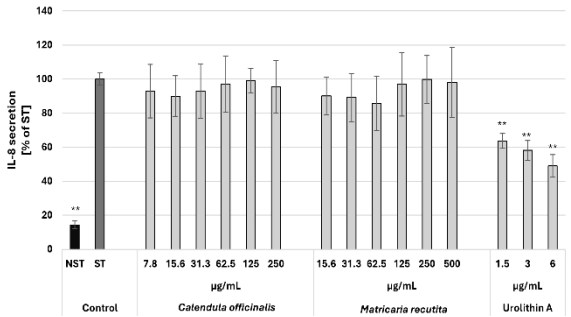

Fig.12. Effect on IL-8 release in HaCaT cells stimulated with a TNF-α/IFN-γ mixture (10 ng/mL each).

A statistically significant decrease (*p < 0.05; **p < 0.001) was observed compared with the stimulated control.

3.5.2. Modulation of IL-6 and IL-8 secretion in NHDF fibroblasts

To assess the anti-inflammatory effects of the tested extracts in dermal fibroblasts, NHDF cells were stimulated with lipoteichoic acid (LTA), a Toll-like receptor 2 agonist derived from Gram-positive bacteria, known to induce IL-6 and IL-8 secretion.

Both extracts demonstrated a clear dose-dependent inhibitory effect on IL-6 and IL-8 secretion **(Fig. 13-14).** At high concentrations (125 – 250 µg/mL) of *Calendula officinalis* extract, the levels of both cytokines decreased to 20-30% of stimulated control. *Matricaria recutita* extract also suppressed cytokine secretion, with high doses (250-500 µg/mL) causing profound suppression of IL-6 and IL-8 to 15-30% of stimulated control. However, for IL-6 at 15.6 µg/mL, a biphasic response was observed: the value exceeded stimulated control by almost 20%, whereas for IL-8 at the same dose, the effect was close to control.

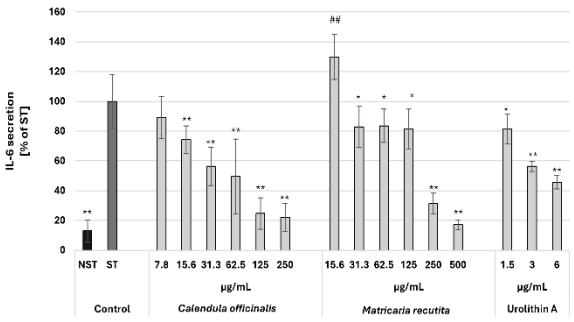

Fig. 13. Effect on IL-6 release in NHDF cells stimulated with LTA (10 ng/mL). A statistically significant increase (#p < 0.05; ##p <0.001) or decrease (*p < 0.05; **p < 0.001) was observed compared with stimulated control.

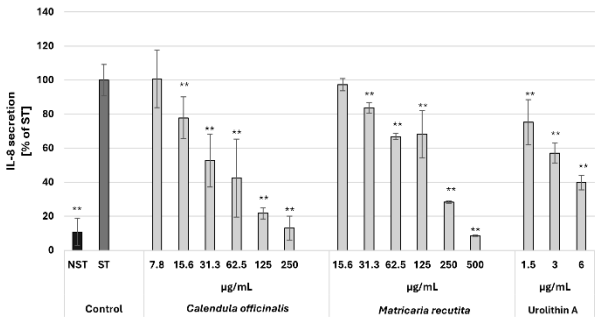

Fig. 14. Effect on IL-8 release in NHDF cells stimulated with LTA (10 ng/mL). A statistically significant decrease (*p < 0.05; **p < 0.001) was observed compared with the stimulated control.

4. Conclusions

Calendula officinalis and *Matricaria recutita* extracts, characterized by distinct phytochemical profiles, demonstrated a complex yet balanced interaction with both skin microbiota and dermal cells. The marigold flower extract (MFE), rich in phenolics, flavonoids, and saponins, and the chamomile flower extract (CFE), containing mainly flavonoids and caffeic acid derivatives, both remained chemically stable under microbiota exposure, as no new metabolites were identified after incubation with human skin microbial communities. This stability indicates a resistance of the major constituents to microbial degradation, suggesting that their biological effects arise primarily from native phytochemicals rather than microbiota-derived metabolites.

Chamomile extract induced donor-dependent changes, with certain samples showing increased richness and diversity compared with the control, reflecting a more variable and individualized modulatory potential. In contrast, marigold extract consistently reduced richness and diversity, resulting in a more uniform microbial structure. Importantly, neither extract caused collapse of the microbial ecosystem; instead, they selectively modulated the relative abundance of dominant and subdominant taxa while preserving overall community complexity. Such selective remodeling may represent a beneficial ecological mechanism, supporting skin homeostasis through microbiota rebalancing rather than broad-spectrum antimicrobial activity.

Moreover, the observed decrease in the relative abundance of *Staphylococcaceae, Corynebacteriaceae,* and *Enterococcaceae* suggests a potential anti-inflammatory rebalancing of the skin microbiota, as these taxa are often associated with dysbiosis and inflammatory skin conditions. Concurrently, the increase in unclassified *Bacillales* and *Bacillaceae* may indicate the enrichment of species with antimicrobial or immunomodulatory properties, contributing to a more resilient and less pro-inflammatory microbial ecosystem. The reduction in unclassified bacteria and *Pseudomonadaceae*, which include opportunistic and pro-inflammatory species such as *Pseudomonas aeruginosa,* further supports the hypothesis of a decreased pathogenic and inflammatory potential.

At the cellular level, both extracts showed favorable biocompatibility with human skin cells at a concentration of ≤ 250 µg/mL. Fibroblasts appeared more resilient and responsive to low-dose stimulation, while keratinocytes displayed higher sensitivity to concentrated treatments. *C. officinalis* showed a clear dose-dependent response in keratinocytes: higher concentrations were cytotoxic, intermediate levels promoted cell proliferation, and the lowest doses produced no measurable traditional application in wound healing and tissue repair. In contrast, *M. recutita* showed a stabilizing and cytoprotective profile, helping to maintain cellular homeostasis without inducing excessive proliferation or stress responses.

Summarizing, these findings emphasize a dual mechanism of action: direct cellular modulation and indirect microbiota-mediated balance. The extracts act as gentle regulators – stabilizing the skin microbial ecosystem while simultaneously protecting and modulating inflammatory responses in skin cells. Notably, the relative abundance of potentially pro-inflammatory and opportunistic taxa decreased, whereas beneficial and immunomodulatory groups increased. This selective microbial modulation reflects a shift toward a more balanced, resilient, and anti-inflammatory skin environment. This dual interaction between phytochemicals, microbiota, and host cells provides a mechanistic basis for the traditional therapeutic efficacy

of *Calendula officinalis* and *Matricaria recutita* and highlights their potential as multifunctional components in formulations aimed at restoring skin health and homeostasis.

Appendix

List of abbreviations:

CFE chamomile flower extract

BLAST basic local alignment search tool

DMEM Dulbecco's modified Eagle medium

DPBS Dulbecco's phosphate-buffered saline

FBS fetal bovine serum

HaCaT human epidermal keratinocyte line

MFE marigold flower extract

NHDF normal human dermal fibroblasts

NST non-stimulated control

IL interleukin

ST stimulated control

SRB sulforhodamine B

ELISA enzyme-linked immunosorbent assay

IFN interferon

TNF tumor necrosis factor

LTA Lipoteichoic acid

UHPLC-DAD-MS ultra-high performance liquid chromatography (UHPLC) coupled to diode array detection (DAD) and multi-stage mass spectrometry (MS)

OTU operational taxonomic unit

PCR polymerase chain reaction

QIME quantitative insights into microbial ecology

UCHIME algorithm for detecting chimeric sequences

VSEARCH versatile open-source tool for metagenomics

Author Contributions: Conceptualization, **N.M.**; methodology, **W.S., J.P.P., S.G.**;investigation, **N.M.;** resources, **S.G.;** data curation, **N.M.;** writing—original draft preparation, **N.M.;** writing—review and editing, **W.S., D.P., S.G.**; visualization, **N.M., D.P.;** supervision, **J.P.P., S.G.**;project administration, **N.M., S.G.**; funding acquisition, **S.G.** All authors have read and agreed to the published version of the manuscript.

Funding: This research was funded by by the National Science Centre Poland grant Preludium Bis 2 No. 2020/39/O/NZ7/01109.

Informed Consent Statement: Informed consent was obtained from all subjects involved in the study.

Acknowledgments: The authors express their sincere gratitude to **Kamila Konstancja Lis**, **Aleksandra Anna Nyczka**, and **Anastasiya Kharyna**, the students of the Department of Pharmaceutical Biology, Medical University of Warsaw, for their valuable assistance in conducting the experiments and data collection

Conflicts of Interest: The authors declare no conflict of interest.

References

1. Richard MA, Paul C, Nijsten T, et al. Prevalence of most common skin diseases in Europe : a population-based study. *J Eur Acad Dermatology Venerelogy* **2022**; *1088–1096*. DOI: 10.1111/jdv.18050

2. Hoffmann AR. The cutaneous ecosystem : the roles of the skin microbiome in health and its association with inflammatory skin conditions in humans and animals. V*et Dermatol* **2017***; 28: 60-e15*. DOI: 10.1111/vde.12408

3. Simmons J, Gallo RL. The Central Roles of Keratinocytes in Coordinating Skin Immunity. *J Invest Dermatol* **2024**; *144: 2377-2398*. DOI: 10.1016/j.jid.2024.06.1280

4. Atit R, Thulabandu V, Chen D. Dermal fibroblast in cutaneus development and healing. *Wiley Interdiscip Rev Dev Biol* **2018***; 7: 1-19*. DOI: 10.1002/wdev.307.Dermal

5. Khan H. Medicinal Plants in Light of History : Recognized Therapeutic Modality. *J Evidence-Based Compementary Altern Med* **2014**; *19: 216-219*. DOI: 10.1177/2156587214533346

6. Marelli M. Medicinal Plants. Plants 2021; 10. DOI: 10.3390/plants10071355

7. Proestos C. The Benefits of Plant Extracts for Human Health. *Foods* **2020**; *10-12*. DOI: 10.3390/plants10071355

8. Khumaidi A, Murwanti R, Damayanti E, et al. Empirical use, phytochemical, and pharmacological effects in wound healing activities of compounds in Diospyros leaves: A review of traditional medicine for potential new plant-derived drugs Akhmad Khumaidi. *J Ethnopharmacol* **2025**; *337*. DOI: 10.1016/j.jep.2024.118966

9. Fernandes A, Rodrigues PM, Pintado M, et al. Phytomedicine A systematic review of natural products for skin applications : Targeting inflammation , wound healing , and photo-aging. *Phytomedicine* **2023**; *115*. DOI: 10.1016/j.phymed.2023.154824

10. Nicolaus C, Junghanns S, Hartmann A, et al. In vitro studies to evaluate the wound healing properties of *Calendula officinalis* extracts. *J Ethnopharmacol* **2017**; *196*. DOI: 10.1016/j.jep.2016.12.006

11. Santos DS dos, Barreto R de SS, Serafini MR, et al. Phytomedicines containing *Matricaria species* for the treatment of skin diseases: A biotechnological approach. *Fitoterapia* **2019**; *138*. DOI : 10.1016/j.fitote.2019.104267

12. Flemming M, Kraus B, Rascle A, et al. Revisited anti-inflammatory activity of matricine in vitro: Comparison with chamazulene. *Fitoterapia* **2015**; *106*: *122–128*. DOI: 10.1016/j.fitote.2015.08.010

13. Krizkovska B, Hoang L, Brdova D, et al. Modulation of the bacterial virulence and resistance by well-known European medicinal herbs. *J Ethnopharmacol* **2023**; *312*. DOI: 10.1016/j.jep.2023.116484

14. Skowrońska W, Pawłowska KA, Obrębski M, et al. Chemical composition, skin microbiota metabolism, antimicrobial potential and anti-inflammatory properties of witch hazel bark (*Hamamelis virginiana* L.). *J Ethnopharmacol* **2025**; *353*: *120433*. DOI: 10.1016/j.jep.2025.120433

15. Piwowarski JP, Granica S, Zwierzyńska M, et al. Role of human gut microbiota metabolism in the anti-inflammatory effect of traditionally used ellagitannin-rich

plant materials Jakub P. Piwowarski. *J Ethnopharmacol* **2014**; *155*: *801–809*. DOI: 10.1016/j.jep.2014.06.032

16. Polish Pharmacopoeia, 12th Edition. Monograph 04/2020:1297 *Calendulae flos* , Warsaw: Office for Registration of Medicinal Products, Medical Devices and Biocidal Products; 2020.

17. Polish Pharmacopoeia, 12th Edition. Monograph 07/2019:0404 *Matricariae flos* , Warsaw: Office for Registration of Medicinal Products, Medical Devices and Biocidal Products; 2020.

18. Edgar RC, Haas BJ, Clemente JC, et al. UCHIME improves sensitivity and speed of chimera detection. *Bioinformatics* **2011**; *27: 2194–2200*. DOI : 10.1093/bioinformatics/btr381

19. Rognes T, Flouri T, Nichols B, et al. VSEARCH: A versatile open source tool for metagenomics. *PeerJ* **2016**; *1–22*. DOI: 10.7717/peerj.2584

20. Eren AM, Esen C, Quince C, et al. Anvi'o : an advanced analysis and visualization platform for 'omics data. *PeerJ* **2015**; *1–29*. DOI: 10.7717/peerj.1319

21. Chao A, Chiu C. Species Richness : Estimation and Comparison. *Wiley StatsRef Stat Ref Online* **2014**; DOI: 10.1002/9781118445112.stat03432.pub2

22. Thukral AK. A review on measurement of Alpha diversity in biology. *Agric Res J* **2017**; *54: 1–10*. DOI: 10.5958/2395-146X.2017.00001.1

23. Olennikov DN, Kashchenko NI, Chirikova NK. Isorhamnetin and Quercetin Derivatives as Anti-Acetylcholinesterase Principles of Marigold (*Calendula officinalis*) Flowers and Preparations. *Int J Mol Sci* **2017**; *18: 1–17*. DOI: 10.3390/ijms18081685

24. Skowrońska W, Granica S, Piwowarski JP, et al. Wound healing potential of extract from *Sambucus nigra* L. leaves and its fractions. *J Ethnopharmacol* **2024**; *320*. DOI: 10.1016/j.jep.2023.117423

25. Budan A, Bellenot D, Freuze I, et al. Potential of extracts from *Saponaria officinalis* and *Calendula officinalis* to modulate in vitro rumen fermentation with respect to their content in saponins. *Biosci Biotechnol Biochem* **2014**; *78: 288–295*. DOI : 10.1080/09168451.2014.882742

26. Liu J, Guo Y, Zhang J, et al. Phytomedicine Systematic chemical analysis of flavonoids in the Nelumbinis stamen. *Eur J Integr Med* **2014**; *21: 1753–1758*. DOI : 10.1016/j.phymed.2014.09.003

27. Tsivelika N, Irakli M, Mavromatis A, et al. Phenolic Profile by HPLC-PDA-MS of Greek Chamomile Populations and Commercial Varieties and Their Antioxidant Activity. *Foods* **2021**; DOI: :10.3390/ foods10102345

28. Lin L, Harnly JM. LC-PDA-ESI/MS Identification of the Phenolic Components of Three *Compositae Spice*s: Chamomile, Tarragon, and Mexican Arnica. *Nat Prod Commun* **2012**; *7: 749–752*

29. Caleja C, Barros L, Amilcar LA, et al. Development of a functional dairy food : Exploring bioactive and preservation effects of chamomile (*Matricaria recutita* L .). *J Funct Foods* **2015**; *16: 114–124*. DOI: 10.1016/j.jff.2015.04.033

30. Luan Y, Cui J, Zhai J. High-throughput sequencing reveals differential expression of miRNAs in tomato inoculated with *Phytophthora infestans*. *Planta* **2015**; *1405–1416*. DOI: 10.1007/s00425-015-2267-7

31. Melnyk N, Popowski D, Strawa JW, et al. Skin microbiota metabolism of natural products from comfrey root (*Symphytum officinale* L .). *J Ethnopharmacol* **2024**; *318*. DOI: 10.1016/j.jep.2023.116968

32. Orellana EA, Kasinski AL. Sulforhodamine B (SRB) Assay in Cell Culture to Investigate Cell Prolifiration. *Bio Protoc* **2016**; *6*. DOI: 10.21769/BioProtoc.1984.Sulforhodamine

33. Vichai V, Kirtikara K. Sulforhodamine B colorimetric assay for cytotoxicity screening. *Nat Protoc* **2006**; *1: 1112–1116*. DOI: 10.1038/nprot.2006.179

34. Verma PK, Raina R, Agarwal S, et al. Phytochemical ingredients and pharmacological potential of *Calendula officinalis* Linn. *Pharm Biomed Res* **2018**; *4: 1–17*. DOI: 10.1007/s11101-005-4053-9

35. Mihyaoui A El, Esteves JCG, Charfi S, et al. Chamomile (*Matricaria chamomilla* L .): A Review of Ethnomedicinal Use , Phytochemistry and Pharmacological Uses. *Life* **2022**; *12: 1–41*. DOI: 10.3390/life12040479

36. Dong L, Lee H, Liu Z, et al. Anti-Inflammatory Activity of Compounds Isolated from *Digitalis purpurea* L . in TNF- α / IFN- γ -Induced HaCaT Keratinocytes and a Three-Dimensionally Reconstructed Human Skin Model. *Molucular Sci* **2022**; *26: 1088–1069*. DOI: 10.3390/ijms26167747

37. Grebenciucova E, Vanhaerents S. Interleukin 6 : at the interface of human health and disease. *Front Immunol* **2023**; *6: 1–10*. DOI: 10.3389/fimmu.2023.1255533

38. Prokop A, Magiera A, Olszewska MA. Proanthocyanidins as Therapeutic Agents in Inflammation - Related Skin Disorders. *Int J Mol Sci* **2025**; DOI: 10.3390/ijms262010116

39. Clausen ML, Kezic S, Olesen CM, et al. Cytokine concentration across the stratum corneum in atopic dermatitis and healthy controls. *Sci Rep* **2020**; *2–9*. DOI: 10.1038/s41598-020-78943-6

40. Zheng Z. Cellular and Molecular Mechanisms of Phytochemicals Against Inflammation - Associated Diseases and Viral Infection. *Cell Biol Int* **2025**; *606–633*. DOI: 10.1002/cbin.70011

41. Kopalli SR, Annamneedi VP, Koppula S. Potential Natural Biomolecules Targeting JAK / STAT / SOCS Signaling in the Management of Atopic Dermatitis. *Molecules* **2022**; *27: 1–23*. DOI: 10.3390/molecules27144660

42. Yin Q, Wang L, Yu H, et al. Pharmacological Effects of Polyphenol Phytochemicals on the JAK-STAT Signaling Pathw. *Front Pharmacol* **2021**; *12*. DOI: 10.3389/fphar.2021.716672